THE JOURNAL OF PHYSICAL CHEMISTRY B

Article

pubs.acs.org/JPCB

Fluid and Resistive Tethered Lipid Membranes on Nanoporous Substrates

Gautam Gupta,[*,†,‡] Kyle Staggs,[†] Aditya D. Mohite,[†,‡] Jon K. Baldwin,[†] Srinivas Iyer,[§] Rangachary Mukundan,[‡] Amit Misra,[†] Antonia Antoniou,[∥] and Andrew M. Dattelbaum[*,†,‡]

[†]Center for Integrated Nanotechnologies, [‡]MPA-11, Materials Synthesis and Integrated Devices, and [§]B-11, Bioenergy and Biome Sciences, Los Alamos National Laboratory, Los Alamos, New Mexico 87545, United States

[∥]School of Mechanical Engineering, Georgia Institute of Technology, Atlanta, Georgia 30332, United States

Supporting Information

ABSTRACT: Cell membranes perform important biological roles including compartmentalization, signaling, and transport of nutrients. Supported lipid membranes mimic the behavior of cell membranes and are an important model tool for studying membrane properties in a controlled laboratory environment. Lipid membranes may be supported on solid substrates; however, protein and lipid interactions with the substrate typically result in their denaturation. In this report, we demonstrate the formation of intact lipid membranes tethered on nanoporous metal thin films obtained via a dealloying process. Uniform lipid membranes were formed when the surface defect density of the nanoporous metal film was significantly reduced through a two-step dealloying process reported here. We show that the tethered lipid membranes on nanoporous metal substrates maintain both fluidity and electrical resistivity, which are key attributes to naturally occurring lipid membranes. The lipid assemblies supported on nanoporous metals provide a new platform for investigating lipid membrane properties, and potentially membrane proteins, for numerous applications including next generation biosensor platforms, targeted drug-delivery, and energy harvesting devices.

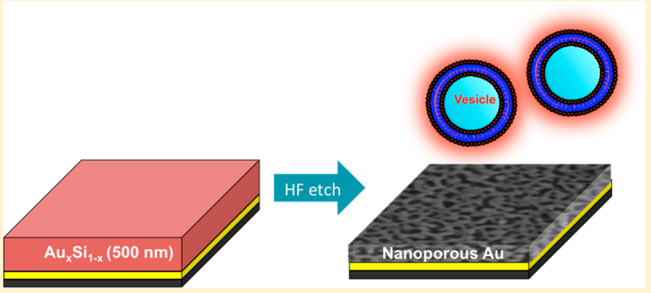

INTRODUCTION

Cell membranes are composed of two or more leaflets of organized phospholipids that are fluid and impermeable to ions. Black lipid membranes,[1] liposomes,[2] and solid supported membranes (SSMs)[3,4] are model lipid systems used to mimic cell membranes found in nature. Among these systems, SSMs exhibit high stability and are often used to characterize lipid membrane dynamics, for example, membrane fluidity, membrane resistivity, and as a support to incorporate transmembrane proteins (TMPs).[5] However, use of these systems to study incorporated transmembrane proteins has had limited success due to denaturing interactions with the substrates.[3] To overcome these interactions, researchers have used polymer cushions,[6] lipids tethered to supports through spacer units,[5] as well as porous substrates[7−9] to support lipid membranes. It is essential to understand the formation of lipid membranes on substrates, and the resulting membranes should possess both fluidity and have optimal resistance before incorporation of transmembrane proteins is conducted.

Here we investigate the use of nanoporous metal films as platforms for supporting lipid membranes because the surface porosity can potentially minimize denaturing interactions between integral membrane proteins. Further, the metal film can act as a conducting electrode to help characterize resistivity properties of the supported membrane that are important if membrane ion-channel proteins are to be studied. Among the different nanoporous film platforms available, nanoporous alumina films coated with a thin gold layer developed by Steinem and co-workers, as well as others, have been effective for electrochemical characterization of tethered lipid membranes.[10−13]

Nanoporous metals prepared by dealloying have recently received significant attention as they have high surface area per unit volume, have exceptional mechanical strength, and are relatively straightforward to prepare.[14−19] Typically, nanoporous metals are formed by selective dissolution of a less noble metal such as Ag from a homogeneous alloy of, for example, Ag/Au in an acidic environment resulting in the formation of bicontinuous interpenetrating ligaments of the more noble metal, Au in this case, with a variable pore size.[14,20,21] We have recently reported an alternative process to prepare nanoporous metal films that are highly stable.[19,22,23] Such porous conductive matrices are attractive candidates for next generation materials for applications in a number of fields including fuel cells,[24,25] catalysts,[24−26] actuators,[27] plasmonics,[28] biosensors,[29] and photovoltaics.[30]

In this paper, we report for the first time to our knowledge formation of tethered lipid membranes on codeposited Au−Si

Received: May 10, 2015
Revised: August 23, 2015

ACS Publications © XXXX American Chemical Society

DOI: 10.1021/acs.jpcb.5b04482
J. Phys. Chem. B XXXX, XXX, XXX−XXX

films and dealloyed nanoporous films. To form uniform and continuous supported lipid membranes, we modified the dealloying processing conditions to prepare pit/crack free nanostructured films. Lipid compositions were varied to yield resistive and fluid lipid membranes on nanoporous supports. Fluorescence recovery after photobleaching (FRAP) measurements and correlated impedance measurement studies indicate that both the type of nanoporous architecture and the choice of lipid membrane are essential to obtain intact phospholipid membranes. These architectures will be useful for realization of lipid membrane based sensors, actuators, energy harvesting devices, and drug-delivery platforms.[30,31]

EXPERIMENTAL METHODS

Materials. Silicon substrates (test grade; p-doped) were purchased from Silicon Sense. Pure (99.99%) gold and silicon were purchased from Goodfellow. HEPES buffer, HF, and other chemicals were used as received from Fischer Scientific. 1-Palmitoyl-2-oleoyl-*sn*-glycero-3-phosphocholine (POPC), 1,2-dipalmitoyl-*sn*-glycero-3-phosphothioethanol (DPPTE), and 1-oleoyl-2-6-[(7-nitro-2-1,3-benzoxadiazol-4-yl)amino]-hexanoyl-*sn*-glycero-3-phospho ethanol amine (NBDPE) were obtained from Avanti Polar Lipids and used without further purification.

Preparation of Substrates. The materials were deposited in a high vacuum electron beam evaporator with a base pressure of $>5.0 \times 10^{-9}$ Torr. Initially, a 1 nm adhesive layer of titanium was deposited onto a clean silicon (100) substrate followed by deposition of a 40 nm Au layer, which acts as an "etch stop" layer during etching experiments. Au and Si were then codeposited using e-beam deposition in the same evaporation chamber with a ratio of ∼20:80 onto the substrates. X-ray fluorescence was used to quantitatively identify the $Au_{20}Si_{80}$ ratio and film thickness. Nanoporous gold substrates were prepared by placing the codeposited substrates in a 2% HF bath and applying a constant voltage of 0.7 V vs Ag/AgCl for 1 min. The structure of the codeposited films and dealloyed films was studied in more detail using scanning electron microscopy (SEM). A two-step etching procedure was also developed to synthesize nanoporous gold films with a more uniform pore size distribution. In the two-step process, a codeposited film was first placed in a 0.1% HF solution for 1 h, followed by a 15−30 min dip in a 1% HF solution. In all cases, substrates were cleaned by rinsing in ethanol, drying under nitrogen, then exposing to UV light (185−254 nm) before deposition of lipid bilayers. The cleaned samples were very hydrophilic with a contact angle of less than 20°.

SEM Imaging. The structure and morphology of the codeposited and dealloyed nanoporous films were obtained by scanning electron microscopy (SEM) using a FEI Quanta 400 instrument with field emission gun (FEG) (FEI Instruments) operated at accelerating voltages of 5 and 10 kV, respectively. Low magnification images provide information about the presence and extent of microscopic pitting in the sample. High magnification images provide information on the nanoporous morphology of the films. Nanoporous gold is highly conductive, and sputtering of a thin metal film was not required for measurements.

Formation of Lipid Assemblies on Substrates. Unilamellar vesicles were prepared using standard extrusion procedures. Briefly, lipids were mixed in appropriate concentration in chloroform solution. The chloroform was evaporated using nitrogen and the resulting dried lipid film was dried in vacuum for at least 30 min. A volume of 1 mL of buffer solution (10 mM HEPES with 50 mM NaCl) was added to rehydrate the lipid film, which was allowed to equilibrate for 1 h above the phase transition temperature of the lipids (20 °C for POPC and 60 °C for vesicles containing DPPTE). The solution was vortexed immediately for 2 min to ensure complete mixing. The solution was then extruded through a 100 nm filter at a temperature above the lipid phase transition. The final concentration of lipids in the liposomes was 1 mg/mL with 1 mol % fluorescent lipid. Typically, vesicles were prepared in the following ratios: (a) 99% POPC with 1 mol % NBDPE and (b) 59.5% DPPTE 39.5% POPC and 1% NBDPE. Lipid assemblies were then prepared by depositing vesicles on porous/nonporous substrates at a desired temperature (20 °C for POPC and 60 °C for vesicles containing DPPTE) for 0.5−1 h.

Fluorescence Recovery after Photobleaching. Fluorescence images were collected on an Olympus microscope equipped with an NBD filter set from Chroma Technology Corp along with an ORCA-ER (model LB10-232, Hamamatsu Corporation, Bridgewater, NJ). A Hg lamp as the light source was used to visualize all fluorescent samples. Two filter wheels, one containing a set of excitation and the other emission filters, were mounted in front of the light source and the CCD camera, respectively. An extra triple band emitter was installed in the dichroic mirror cube for aiding in focusing through the eyepiece. Typically, the lipid membranes were obtained via adsportion of vesicles with a desired lipid composition on codeposited or nanoporous substrates. The samples were rinsed repeatedly for 10 times. FRAP measurements were conducted immediately after assembly. Briefly, a spot was exposed to intense fluorescence and bleached. Recovery of fluorescence due to lateral mobility of lipids was observed over desired amount of time. We used a simplified method reported by Yguerabide et al. to estimate the diffusion coefficient and the percentage recovery.[32]

Electrochemical Measurements. Electrochemical measurements were performed in a three-electrode setup using a custom designed electrochemical cell with Ag/AgCl as the reference electrode and a platinum wire as a counter electrode. A CHI potentiostat equipped with a frequency generator was used for impedance measurements. All electrochemical measurements were performed in HEPES buffer with 50 mM NaCl. The geometrical surface area of the substrate exposed to aqueous solution was 0.7 cm^2 approximately.

Ellipsometry. Multiple-wavelength ellipsometric optical thickness measurements on the lipid membranes were performed on a spectroscopic ellipsometer (J.A. Woollam, Lincoln, NE, model M-44), set to a nominal incidence angle of 70° from the surface normal, with the exact angle fitted WVASE, J.A. Woollam in a Teflon liquid cell. Lipid vesicles were added to the assembled cell followed by a 30 min wait. The cell was rinsed several times before performing the measurements. Measurements were conducted from 300 to 800 nm, and modeling was performed using WVASE software (J. A. Woollam Co., Lincoln, NE). The fit quality was assessed using the root-mean-square error (RMSE) between the measured and modeled ellipsometric constants Δ and Ψ over all measured wavelengths. The lipid films were modeled as a single layer of variable thickness, with a refractive index given by the Cauchy parameters.

Electrochemical Impedance Spectra Modeling. The electrochemical impedance spectra were modeled using Zview software. For all data, a simple R(CPE-R) model was initially

DOI: 10.1021/acs.jpcb.5b04482
J. Phys. Chem. B XXXX, XXX, XXX−XXX

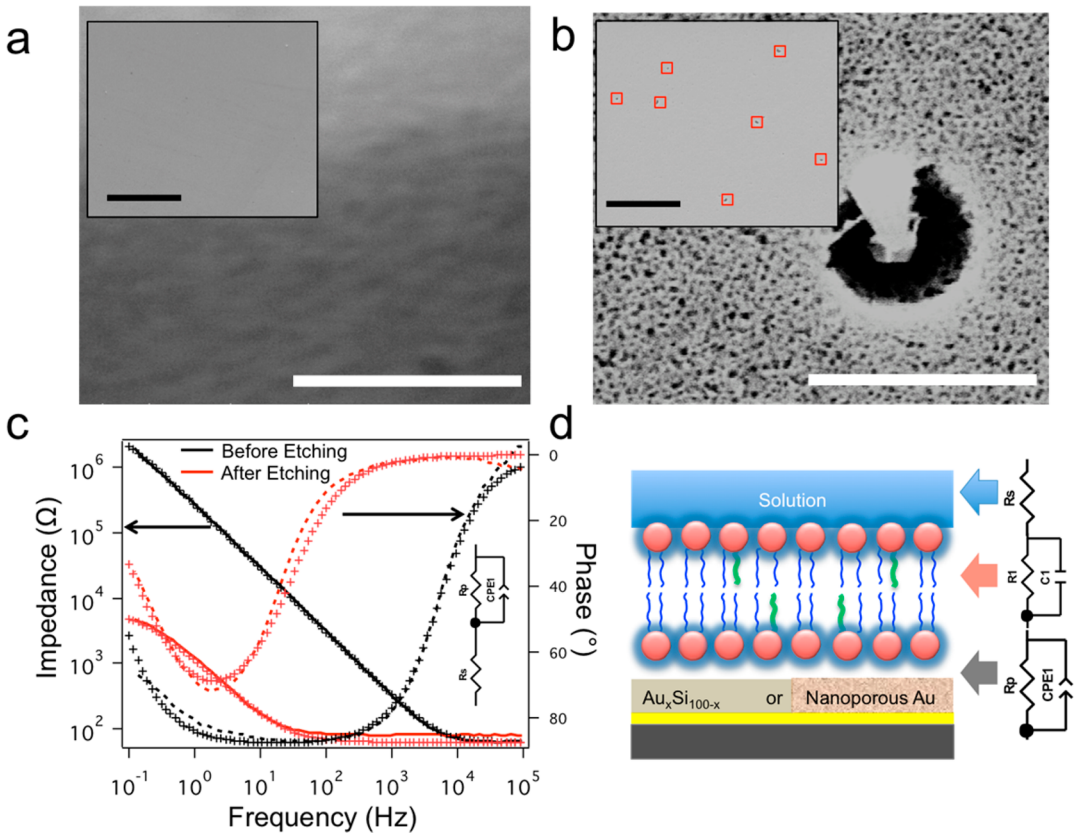

Figure 1. (a) SEM image of an isotropic, nonporous codeposited $Au_{20}Si_{80}$ alloy film. A low- resolution SEM image of the surface is shown in the inset. (b) SEM image of a typical nanoporous gold film synthesized using electrochemical etching (0.7 V in 2% HF bath). The red boxes in the inset highlight pitting in the surface. (c) Electrochemical impedance spectra (Bode plot) of the codeposited $Au_{20}Si_{80}$ film before (black lines) and after (red lines) HF etching. Solid lines correspond to the impedance data, while dashed lines correspond to the phase data versus frequency. "+" symbols are the results of the fitting procedure with the equivalent circuit diagram obtained from Zview. (d) Schematic of a lipid assembly on a codeposited $Au_{20}Si_{80}$ substrate, as well as a nanoporous substrate, and the corresponding equivalent circuit diagram. Scale bar = 500 nm; inset scale bar = 5 μm.

used followed by addition of Warburg impedance to the equivalent circuit diagram.

RESULTS AND DISCUSSION

Characterization of Codeposited and Nanoporous Substrates. The morphology and electrochemical characterization of the initial codeposited Au_xSi_{1-x} film (typically, $x = 0.2$ unless stated otherwise) and dealloyed nanoporous metal substrates was performed prior to deposition of a lipid membrane.

Initial investigation was made with codeposited substrates with variable composition, namely Au_9Si_{91}, $Au_{19}Si_{81}$, $Au_{28}Si_{72}$, and $Au_{41}Si_{59}$ respectively. These different compositions were subsequently etched resulting in nanoporous substrates, which possess variable pore size and ligament distribution. The 9% Au samples had very large pore size and increased roughness and therefore not suitable for formation of lipid membranes upon adsorption of vesicles which are approximately 100 nm in size, where as 40% gold samples led to retention of gold atoms due to incomplete etching, and presence of less number of pores.[19] Therefore, $Au_{20}Si_{80}$ films (~500 nm) were utilized and the substrates were prepared by codeposition of Au and Si using an electron beam assisted deposition technique described previously.[19,22,23] A Ti adhesive layer (~10 nm) and a thin layer (~40 nm) of Au, which serves as an "etch-stop", were also deposited beneath the Au_xSi_{1-x} films. The codeposited substrates were found to be isotropic in nature although some surface roughness was observed by scanning electron microscopy (SEM) as shown in Figure 1a. Dealloying of silicon from the $Au_{20}Si_{80}$ films was performed in a 2% HF bath by applying a single step-potential of 0.7 V for 60s. The Au "etch-stop" layer prevents etching of silicon from the substrate, as well as delamination of the film. Electrochemical etching selectively removes silicon resulting in a continuous porous structure with variable pore sizes ranging from 5 to 40 nm as seen in Figure 1b. However, typically several "large" ~0.5−1 μm diameter "pits" are observed in the surface (highlighted by red boxes) as also seen in the Figure 1b. Detailed characterization of these nanoporous substrates including the complete removal of silicon, shrinkage of films after dealloying and pore size distribution by altering the metal content has been reported earlier by us in a previous report.[19] Electrochemical impedance spectroscopy (EIS) was used to study the electrical properties of the codeposited films before and after etching of Si. Figure 1c shows the Bode plots obtained from codeposited and nanoporous films. As seen in Figure 1c, there is a dramatic drop in impedance before and after electrochemical etching due to removal of Si from the film. The equivalent circuit used to model the impedance data is shown in Figure 1c and consists of the resistance of solution and wires (Rs) in series with an interfacial constant phase element (CPE) and a polarization resistance (Rp) circuit in parallel. A CPE is a circuit element used to replace a capacitor, and is generally associated with a nonhomogenous surface and variable current density at the

DOI: 10.1021/acs.jpcb.5b04482
J. Phys. Chem. B XXXX, XXX, XXX−XXX

Table 1. Variables Used To Describe an Equivalent Circuit Model to Fit Impedance Data for Nonporous $Au_{20}Si_{80}$ Substrates before and after Exposure to DPPTE:POPC Vesicles[a]

elements	$Au_{20}Si_{80}$	$Au_{20}Si_{80}$ (control/codeposited substrate)	DPPTE:POPC
Rs (ohm)	61.6 (0.91)	32.48 (0.51)	47.3 (F)
Rp (ohm)	3.83×10^6 (3.9)	4.6×10^6 (1.2)	4.8×10^6 (F)
CPE1-T (F)	6.21×10^{-7} (0.89)	2.0×10^{-6} (0.93)	2.0×10^{-6} (F)
CPE1-P (n)	0.9754 (0.14)	0.988 (0.26)	0.988 (F)
R1 (ohm)			2.40×10^7 (1.8)
C1 (F)			2.20×10^{-6} (2.1)

[a]Percent error for each element is reported in parentheses. (F) indicates the parameters that were fixed for the equivalent circuit diagram.

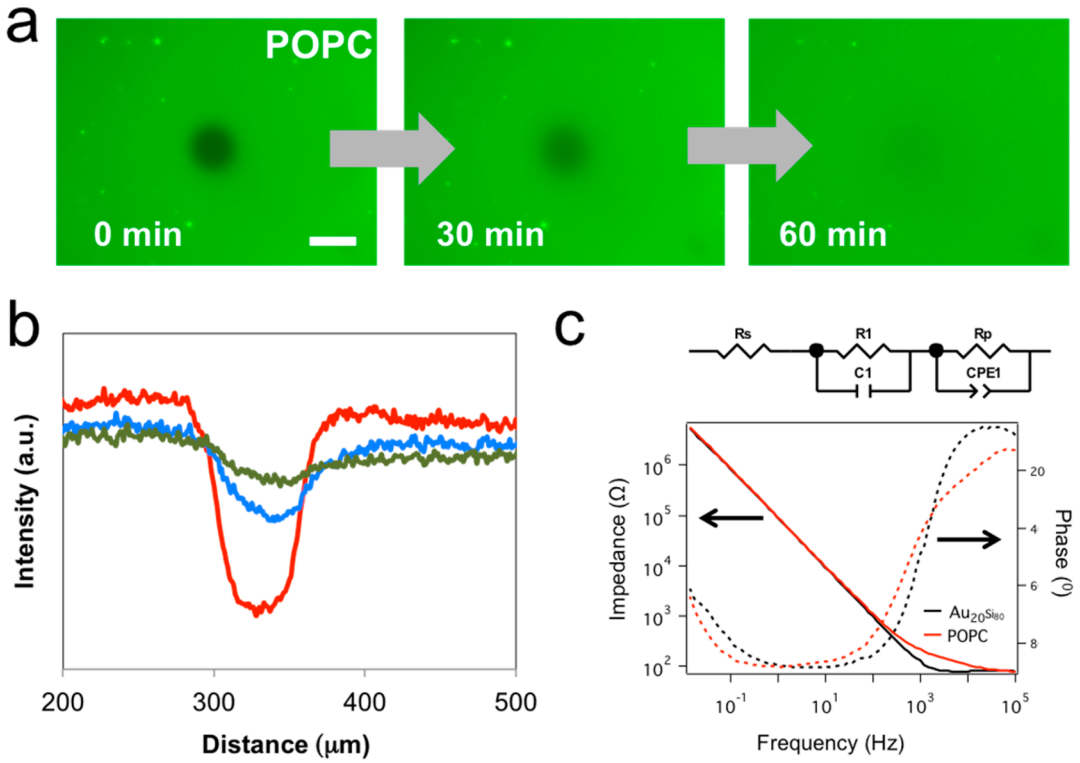

Figure 2. Characterization of lipid POPC:NBDPE (99:1) on codeposited $Au_{20}Si_{80}$ substrates. (a) Time sequential FRAP images of lipid membranes. (b) Intensity profile of corresponding FRAP images (red, t = 0 min; blue, t = 30 min; green, t = 60 min). (c) Electrochemical impedance spectra (Bode plot) of the codeposited $Au_{20}Si_{80}$ film before (black lines) and after (red lines) vesicle adsorption. Solid lines correspond to the impedance data, while dashed lines correspond to the phase data versus frequency. Scale bar = 70 μm.

electrode, which might result in these samples from codeposition of Si and Au. The impedance of CPE is defined as

$$Z_{CPE} = 1(j\omega)^{-n}/Q$$

where Q is the magnitude of the CPE, j is the imaginary unit, ω is the angular frequency, and n is the CPE exponent.

From the circuit analysis (performed using Z-view software) of the codeposited film, the values of Rs, Rp, and CPE that best fit the data were 61.62 Ω, 3.8×10^6 Ω, and 6.2×10^{-7} F, respectively (Table 1). The high resistive nature and low capacitance value for the codeposited substrate may affect our ability to electrochemically detect the formation of a lipid assembly on the codeposited substrates, as the capacitance of a lipid bilayer is similar to the capacitance of the $Au_{20}Si_{80}$ films. Further, an n value of 0.97 for the codeposited substrates indicates only a very slight deviation from normal capacitive behavior as expected (Table 1).

Note that a value of n = 1 indicates the presence of an ideal capacitive layer.[33] Electrochemical etching of the Au_xSi_{1-x} film in HF results in a substantial decrease in the polarization resistance Rp (6.5 KΩ) and an increase in CPE to 1.7×10^{-4} F due to an increase in surface area and removal of silicon (Table 1). After removal of silicon, the surface becomes extremely heterogeneous and a deviation from the ideal capacitor behavior is clearly observed with an n value of 0.88. Thus, this etching process results in a substrate that has low impedance and substantially different capacitance than that of a typical lipid membrane. In addition, the nanoporous substrates prepared in this way were stable in water and no change in electrochemical behavior was observed over a period of several days while stored under PBS buffer.

Formation of Lipid Membranes on Codeposited Substrates. We deposited a solution of lipid vesicles on the resulting substrates to form a lipid membrane on the surfaces. A schematic of a lipid assembly on a codeposited $Au_{20}Si_{80}$ substrate or nanoporous substrate along with an equivalent circuit diagram describing the systems are shown in Figure 1d. We added circuit elements for the resistance (R1) and capacitance (C1) of the lipid bilayer to model the electrochemical behavior in these assembles to the equivalent circuit

DOI: 10.1021/acs.jpcb.5b04482
J. Phys. Chem. B XXXX, XXX, XXX−XXX

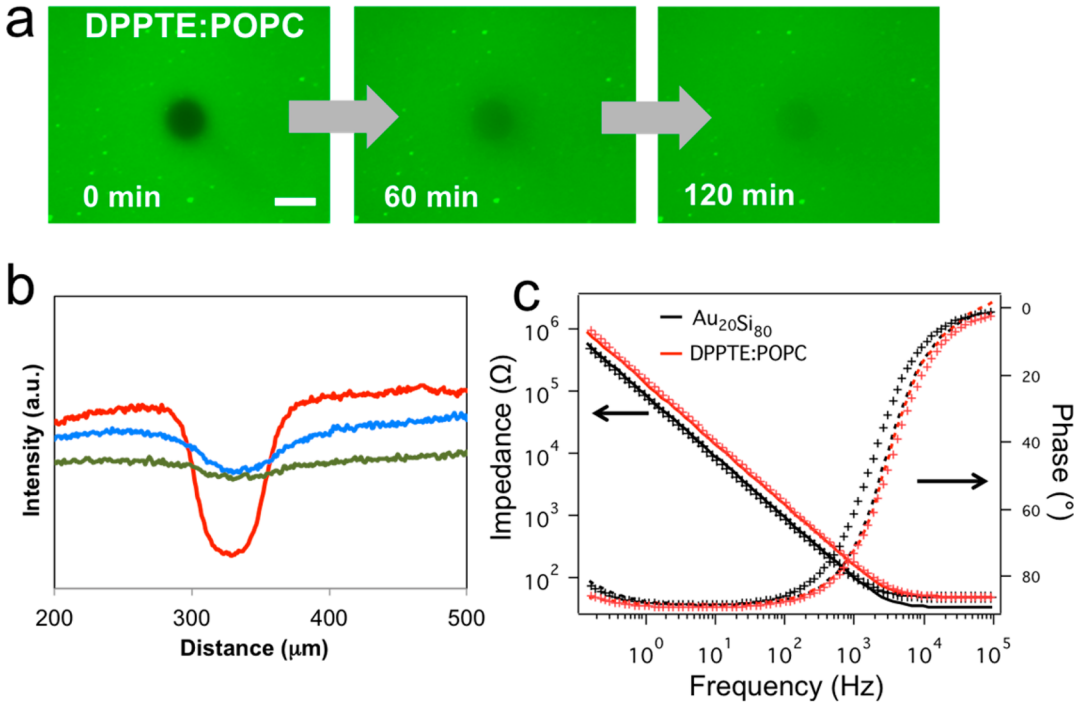

Figure 3. Characterization of DPPTE:POPC:NBDPE (59.5:39.5:1) membranes on codeposited $Au_{20}Si_{80}$ substrates. (a) Time sequential FRAP images of lipid membranes. (b) Normalized intensity profiles of corresponding FRAP images (red, t = 0 min; blue, t = 60 min; green, t = 120 min). (c) Electrochemical impedance spectra (Bode plot) of the codeposited $Au_{20}Si_{80}$ film before (black lines) and after (red lines) vesicle adsorption. Solid lines correspond to the impedance data, while dashed lines correspond to the phase data versus frequency. "+" symbols are the results of the fitting procedure of the equivalent circuit diagram obtained from Zview. Scale bar = 70 μm. "+" symbols are the results of the fitting procedure with the equivalent circuit diagram.

diagram. Initially, we prepared supported lipid membranes on the as-prepared $Au_{20}Si_{80}$ substrates as a baseline measurement that may be compared to lipid membrane formation on the nanoporous metal films. Two lipid vesicle systems were prepared from (a) pure POPC lipids and (b) a mixture of POPC and DPPTE lipids in a 39.5:59.5 mol ratio, respectively. A fluorescent lipid, NBD-PE (1 mol %), was also added for determining membrane fluidity. Initially, pure POPC vesicles were fused onto plasma cleaned codeposited $Au_{20}Si_{80}$ films at room temperature for 30 min. A J. A. Woollam VASE instrument with a liquid cell was used to determine the thickness of the lipid assembly formed on the codeposited film. A thickness of 3.9 nm was observed, which is consistent with formation of a supported POPC bilayer.[34] Because this sample is 80% Si, it is likely covered in many places by SiO_2, which has been used extensively to support lipid bilayers.[35] Having verified lipid bilayer formation, fluorescence recovery after photobleaching (FRAP) experiments were done to characterize membrane fluidity. Fluorescence images collected during a typical FRAP experiment at various time points after bleaching a spot in the POPC membrane are shown in Figure 2a. The POPC bilayers have very uniform fluorescence intensities over large areas (cm^2), though some bright spots are occasionally present that might indicate some physical adsorption of intact fluorescent lipid vesicles. A diffusion constant of $\sim(0.6 \pm 0.05) \times 10^{-8}$ cm^2/s was obtained for POPC bilayers on the codeposited films from an analysis of the intensity profiles as shown in Figure 2b. This diffusion value is lower than the typically reported diffusion constants for POPC lipids in a bilayer on SiO_2 (typically $\sim 1 \times 10^{-8}$ cm^2/s).[36,37] The decreased lipid mobility is attributed to the presence of gold atoms at the surface that can interact with the lipid headgroup.

Formation of lipid assemblies on the codeposited films was also investigated using EIS. As seen in the Bode Plot shown in Figure 2c, there was minimal change in impedance after the fusion of POPC vesicles. The lipid membrane was modeled using a combination of a resistor (R1) and a capacitor (C1) as shown in the inset in Figure 2c. The data indicate that either the POPC bilayer is leaky, that is, allows ions to flow at a measurable level, or the capacitance of the substrate is too similar to the capacitance of the bilayer to observe any changes in capacitance, which is consistent with other reports.[33] We note that Purrucker et al. and others have demonstrated the formation of lipid membranes on doped silicon; however, such supports have relatively high impedance making electrochemical detection of supported lipid membranes a challenging task.[35]

To address this issue, we switched our vesicles to a mixture of POPC and thiol-terminated lipids (DPPTE) that is similar to one used previously by Steinem et al. to prepare tethered lipid membranes on gold coated porous alumina surfaces.[10,38] A fluorescent lipid was again added leading to a final mol ratio of DPPTE:POPC:NBDPE (59.5:39.5:1). In addition to being terminated in a thiol group, DPPTE has two saturated C-16 chains, which increases its gel transition temperature to above 55 °C. Therefore, vesicles prepared with DPPTE were extruded and exposed to substrates above the gel transition temperature. The thickness of the resulting lipid membrane on the codeposited was determined using ellipsometry to be about 44.36 ± 1.12 Å, which is slightly greater than the pure POPC bilayer, but may be attributed to the presence of stiffer and longer DPPTE molecules. A FRAP measurement (fluorescence images and intensity profiles) on this sample is shown in Figure 3b.

DOI: 10.1021/acs.jpcb.5b04482
J. Phys. Chem. B XXXX, XXX, XXX−XXX

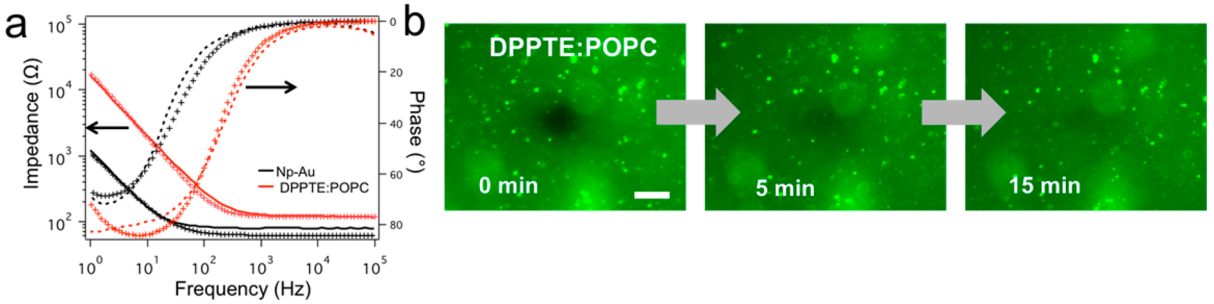

Figure 4. (a) Electrochemical impedance spectra of nanoporous Au obtained via one-step etching before and after vesicle exposure. "+" symbols are the results of the fitting procedure of the equivalent circuit diagram obtained from Zview. (b) FRAP images of a POPC:DPPTE:NBDPE (49.5:49.5:1) lipid assembly on a nanoporous gold substrate. Scale bar = 70 μm. "+" symbols The equivalent circuit diagram used to fit the formation of the lipid membrane includes an additional R1C1 circuit in parallel, while the parameters for the NP-Au remained fixed as shown in Table 2 and SI Figure 3 (R1 = 5.35 × 10^5 Ω, C1 = 9 × 10^{-6} F).

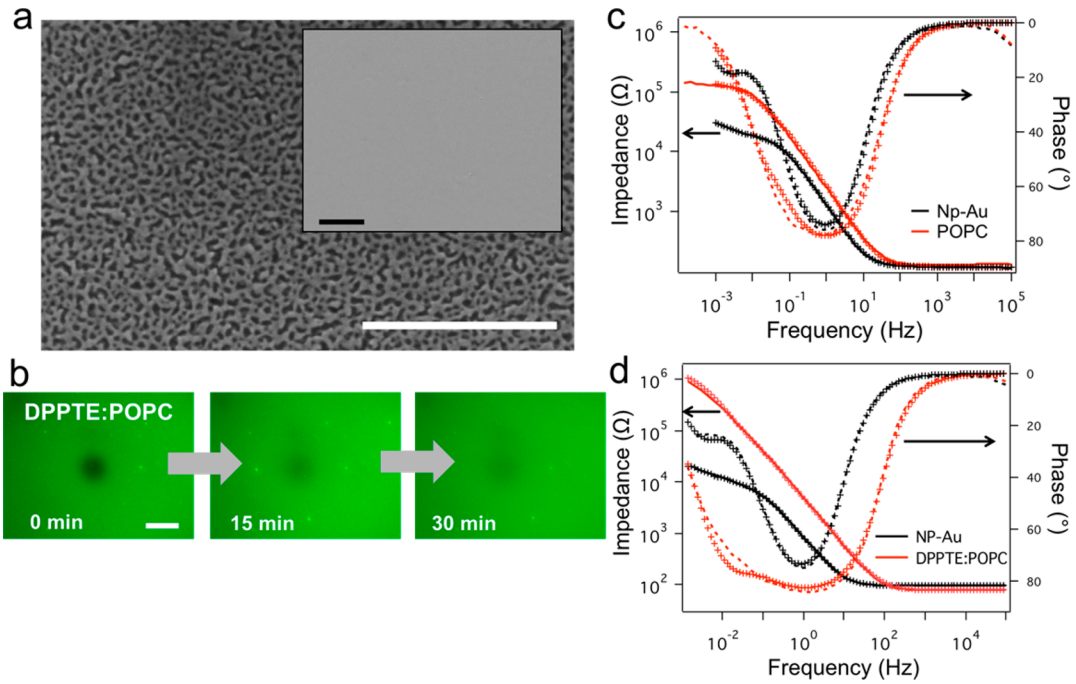

Figure 5. (a) SEM image of a nanoporous gold substrate synthesized using a two-step etching process. A roughly uniform pore size distribution within this sample is observed. Inset shows an SEM image, where no pitting was observed. Scale bar = 500 nm. Inset scale bar = 5 μm. (b) FRAP images of lipid assemblies formed from DPPTE:POPC:NBDPE (59.5:39.5:1) vesicle exposure to nanoporous Au substrates obtained using a two-step etching process. Scale bar = 70 μm. Electrochemical impedance spectra (Bode plots) of nanoporous Au substrates obtained using a two-step etching process. EIS of NP-Au films before and after exposure to (c) POPC:NBDPE vesicles or (d) DPPTE:POPC:NBDPE vesicles. "+" symbols are the results of the fitting procedure of the equivalent circuit diagram obtained from Zview fitting procedure with the equivalent circuit diagram.

The diffusion constant obtained for the DPPTE:POPC lipid bilayer was significantly reduced to (0.06 ± 0.02) × 10^{-8} cm^2/s. The slow rate of diffusion may be attributed to the gel phase of DPPTE found at room temperature, as well as tethering of the DPPTE headgroup on gold. Increasing the temperature to 60 °C during the FRAP experiment does lead to a slightly greater diffusion constant (0.15 x10^{-8} cm^2/s), as expected, but this value remains significantly less than diffusion constant observed for lipids in pure POPC supported membranes. Impedance data from DPPTE:POPC lipid assemblies supported on codeposited $Au_{20}Si_{80}$ films are shown in Figure 3c. In contrast to the POPC membrane, an absolute change in impedance was observed before and after addition of DPPTE:POPC vesicles. Using the same equivalent circuit diagram and fitting routines as described above, we determined the resistance of the lipid membrane to be 2.4 × 10^7 Ω and its capacitance to be 2.2 × 10^{-6} F (Table 1). Thus, these lipid membranes have higher resistance than that of membranes composed of only POPC, indicating a more uniform coverage of an intact supported lipid membrane. These experiments demonstrate that mixtures of POPC and DPPTE can form resistive lipid assemblies tethered on the codeposited $Au_{20}Si_{80}$ substrates; however, lipid mobility in these supported membranes is severely limited.

Formation of Lipid Membranes on Nanoporous Substrates. Based on the above data, we placed lipid vesicles consisting of 59.5% DPPTE, 39.5% POPC, and 1 mol % NBDPE on nanoporous Au substrates. As seen in Figure 4a, there is a significant increase in impedance after vesicle exposure.

This change in impedance is significantly less than what is expected for a lipid membrane spanning the NP−Au surface, indicating incomplete surface coverage of the supported lipid

DOI: 10.1021/acs.jpcb.5b04482
J. Phys. Chem. B XXXX, XXX, XXX−XXX

Table 2. Variables Used To Describe an Equivalent Circuit Model to Fit Impedance Data for Nanoporous Au Substrates before and after Exposure to DPPTE:POPC Vesicles[a]

elements	one-step	DPPTE:POPC	two-step	POPC	two-step	DPPTE:POPC
Rs (ohm)	61 (F)	120 (F)	117.4 (0.4)	117.4 (F)	93.24 (0.25)	77 (F)
Rp (ohm)	6557 (12)	6557 (F)	1.66×10^4 (3.1)	1.66×10^4 (F)	8363 (0.84)	8436 (F)
CPE1-T (F)	0.00017 (5.4)	0.00017 (F)	1.4×10^{-4} (0.90)	1.4×10^{-4}	0.000215 (0.51)	0.000216 (F)
CPE1-P	0.879 (1.8)	0.879 (F)	0.92954 (0.33)	0.92954 (F)	0.9415 (0.19)	0.941 (F)
W1-R			17673 (13.4)	17673 (F)	16625 (8.6)	
W1-T			272 (26)	272 (F)	202 (18.5)	
W1-P			0.4805 (7.2)	0.4805 (F)	0.459 (4.6)	
R2 (ohm)		53469 (21.4)		107320 (2.4)		1.4×10^6 (1.65)
C2 (F)		9.0×10^{-6} (1.79)				
CPE2-T (F)				0.000135 (1.6)		4.44×10^{-5} (0.74)
CPE2-P (n)				0.91986 (0.57)		0.937 (0.23)

[a]One-step and two-step refers to the method of etching used to prepare the nanoporous gold samples. Percent error for each element is reported in the parentheses. (F) refers to the parameters that were fixed for equivalent circuit diagram.

membrane. We were also unable to confirm the thickness of the lipid assembly on the NP-Au substrates using ellipsometry due to the relatively high roughness of the NP-Au film. Others have also observed that rough/porous surfaces affect the formation of continuous supported lipid membranes leading to high capacitance and poor resistive properties.[33] We also tried to characterize these supported membranes using FRAP to investigate the lipid mobility of the film. Fluorescence images (Figure 4b) of these systems exhibit numerous bright spots, which are generally due to intact vesicles on the surface. The rough and irregular surface of the NP-Au films as observed in the SEM (Figure 1b) may cause such poor vesicle fusion. Nevertheless, these supported lipid membranes were found to be fluid at room temperature with a diffusion constant of $(0.8 \pm 0.09) \times 10^{-8}$ cm^2/s, which is significantly faster than lipids in membranes formed on the initial codeposited $Au_{20}Si_{80}$ films. We believe that the terminal thiol of DPPTE acts as a tether to the nanoporous gold surface and a spacer layer to form a better water cushion that allows the POPC and NBD-PE lipids to move more freely throughout the membrane. Lipid mobility may also be rationalized by the water contact angle differences between the substrates. The contact angle for a nonporous $Au_{20}Si_{80}$ film is ~40° while it is ~20° for the NP-Au films. The additional water dragged into the <20 nm pores by capillary action likely causes the drop in contact angle and improves the likelihood of a water cushion between the lipid assembly and nanoporous substrate, which may increase lipid mobility. From these data, it was evident that higher-quality, more uniform nanoporous metal surfaces were required for formation of intact lipid membranes.

Formation of Lipid Membranes on Two-Step Dealloyed Uniform Nanoporous Substrates. To address the challenges of large pitting and surface cracking observed in the nanoporous metal films described above, we modified the etching process to a two-step dealloying process that resulted in more uniform pore size distribution that virtually eliminated pitting over the surface as seen in Figure 5a. In the two-step process, the codeposited substrates are exposed to 0.1% HF for 1 h followed by exposure to a 1% HF solution for 15 or 30 min, resulting in the desired uniform pore structure. Longer exposure times resulted in shrinkage of film thickness, although the pore size distribution was unaltered. We then exposed the nanoporous substrate to vesicles consisting of 59.5% DPPTE, 39.5% POPC, and 1 mol % NBDPE.

As shown in Figure 5b, a very uniform fluorescence image was obtained from the tethered membrane indicating an improved vesicle fusion process. The diffusion constant for these samples was found to be $(0.8 \pm 0.09) \times 10^{-8}$ cm^2/s. EIS data confirms the formation of lipid assemblies on NP-Au films prepared by a two-step etch process. As shown in Figure 5c, an increase in impedance was observed after exposing the NP-Au films to POPC vesicles. Further improvements to the impedance behavior of the lipid membrane were found by fusing DPPTE:POPC vesicles to the NP-Au surface prepared by a two-step etch process. Formation of tethered DPPTE:-POPC assemblies on NP-Au (two-step etch) results in at least a 2 orders of magnitude increase in impedance for several samples. Further, for the DPPTE:POPC tethered membranes, we were able to perform electrochemical measurements at much lower frequencies that allowed us to extract better values to describe this system electrochemically (Figure 5c,d). Impedance curves indicate the diffusion of ions into nanopores when lipid bilayer was not present; therefore, a Warburg diffusion element was introduced into the equivalent circuit model. The supported lipid assembly was modeled using a resistor and a CPE element, and Warburg was removed for fitting the impedance curves, as the lipid bilayer prevents the diffusion of ions into nanopores. The values for the different elements and the models are shown in Table 2. The impedance data along with the FRAP measurements confirm the formation of lipid assemblies on the nanoporous gold films that are both fluid and resistive.

CONCLUSIONS

In summary, we described the formation of lipid membranes supported and tethered on nonporous and nanoporous metal substrates. The lipid membranes formed on the nanoporous substrates are both fluid and highly resistive, thus mimicking two key functional aspects of naturally occurring lipid membranes. The lipid composition of vesicles used to form the supported membranes was critical in realizing the desired properties. Continuous and uniform supported membranes also required higher quality nanoporous gold films that were prepared by a new two-step etching process to make films with minimal cracking and pitting. The lipid assemblies supported on nanoporous Au film described here provide a new platform for investigating lipid membrane properties, and potentially membrane proteins, which may lead to a variety of new architectures for sensing and energy related applications.

DOI: 10.1021/acs.jpcb.5b04482
J. Phys. Chem. B XXXX, XXX, XXX−XXX

■ ASSOCIATED CONTENT

Supporting Information

This material is available free of charge via Internet at The Supporting Information is available free of charge on the ACS Publications website at DOI: 10.1021/acs.jpcb.5b04482.

Details of impedance spectroscopy and models (PDF)

■ AUTHOR INFORMATION

Corresponding Authors

*E-mail: Gautam@lanl.gov.
*E-mail: amdattel@lanl.gov.

Notes

The authors declare no competing financial interest.

■ ACKNOWLEDGMENTS

The authors thank the Center for Integrated Nanotechnologies and Directed Research and Development program at Los Alamos National Laboratory for funding parts of this work. The authors would also like to acknowledge that this work was done, in part, at the Center for Integrated Nanotechnologies, which is an Office of Science user facility.

■ REFERENCES

(1) Boheim, G. Stasistical-Analysis of Alamethicin Channels in Black Lipid Membranes. *J. Membr. Biol.* **1974**, *19*, 277.
(2) Bangham, A. D.; Standish, M. M.; Watkins, J. C. Diffusion of Univalent Ions Across Lamellae of Swollen Phospholipids. *J. Mol. Biol.* **1965**, *13*, 238.
(3) Castellana, E. T.; Cremer, P. S. Solid supported lipid bilayers: From biophysical studies to sensor design. *Surf. Sci. Rep.* **2006**, *61*, 429.
(4) Jass, J.; Tjarnhage, T.; Puu, G. From liposomes to supported, planar bilayer structures on hydrophilic and hydrophobic surfaces: An atomic force microscopy study. *Biophys. J.* **2000**, *79*, 3153.
(5) Wagner, M. L.; Tamm, L. K. Tethered polymer-supported planar lipid bilayers for reconstitution of integral membrane proteins: Silane-polyethyleneglycol-lipid as a cushion and covalent linker. *Biophys. J.* **2000**, *79*, 1400.
(6) Tanaka, M.; Sackmann, E. Polymer-supported membranes as models of the cell surface. *Nature* **2005**, *437*, 656.
(7) Romer, W.; Steinem, C. Impedance analysis and single-channel recordings on nano-black lipid membranes based on porous alumina. *Biophys. J.* **2004**, *86*, 955.
(8) Yang, T.-H.; Yee, C. K.; Amweg, M. L.; Singh, S.; Kendall, E. L.; Dattelbaum, A. M.; Shreve, A. P.; Brinker, C. J.; Parikh, A. N. Optical detection of ion-channel-induced proton transport in supported phospholipid bilayers. *Nano Lett.* **2007**, *7*, 2446.
(9) Werner, J. H.; Montano, G. A.; Garcia, A. L.; Zurek, N. A.; Akhadov, E. A.; Lopez, G. P.; Shreve, A. P. Formation and Dynamics of Supported Phospholipid Membranes on a Periodic Nanotextured Substrate. *Langmuir* **2009**, *25*, 2986.
(10) Drexler, J.; Steinem, C. Pore-suspending lipid bilayers on porous alumina investigated by electrical impedance spectroscopy. *J. Phys. Chem. B* **2003**, *107*, 11245.
(11) Schmitt, E. K.; Nurnabi, M.; Bushby, R. J.; Steinem, C. Electrically insulating pore-suspending membranes on highly ordered porous alumina obtained from vesicle spreading. *Soft Matter* **2008**, *4*, 250.
(12) Studer, A.; Han, X.; Winkler, F. K.; Tiefenauer, L. X. Formation of individual protein channels in lipid bilayers suspended in nanopores. *Colloids Surf., B* **2009**, *73*, 325.
(13) Venkatesan, B.; Polans, J.; Comer, J.; Sridhar, S.; Wendell, D.; Aksimentiev, A.; Bashir, R. Lipid bilayer coated Al2O3 nanopore sensors: towards a hybrid biological solid-state nanopore. *Biomed. Microdevices* **2011**, *13*, 671.
(14) Erlebacher, J.; Aziz, M. J.; Karma, A.; Dimitrov, N.; Sieradzki, K. Evolution of nanoporosity in dealloying. *Nature* **2001**, *410*, 450.
(15) Hakamada, M.; Mabuchi, M. Mechanical strength of nanoporous gold fabricated by dealloying. *Scr. Mater.* **2007**, *56*, 1003.
(16) Mathur, A.; Erlebacher, J. Size dependence of effective Young's modulus of nanoporous gold. *Appl. Phys. Lett.* **2007**, *90*, 061910.
(17) Jia, F. L.; Yu, C. F.; Deng, K. J.; Zhang, L. Z. Nanoporous metal (Cu, Ag, Au) films with high surface area: General fabrication and preliminary electrochemical performance. *J. Phys. Chem. C* **2007**, *111*, 8424.
(18) Erlebacher, J.; Sieradzki, K. Pattern formation during dealloying. *Scr. Mater.* **2003**, *49*, 991.
(19) Gupta, G.; Thorp, J. C.; Mara, N. A.; Dattelbaum, A. M.; Misra, A.; Picraux, S. T. Morphology and porosity of nanoporous Au thin films formed by dealloying of AuxSi1-x. *J. Appl. Phys.* **2012**, *112*, 094320.
(20) Dixon, M. C.; Daniel, T. A.; Hieda, M.; Smilgies, D. M.; Chan, M. H. W.; Allara, D. L. Preparation, structure, and optical properties of nanoporous gold thin films. *Langmuir* **2007**, *23*, 2414.
(21) Lu, X.; Bischoff, E.; Spolenak, R.; Balk, T. J. Investigation of dealloying in Au-Ag thin films by quantitative electron probe microanalysis. *Scr. Mater.* **2007**, *56*, 557.
(22) Antoniou, A.; Bhattacharrya, D.; Baldwin, J. K.; Goodwin, P.; Nastasi, M.; Picraux, S. T.; Misra, A. Controlled nanoporous Pt morphologies by varying deposition parameters. *Appl. Phys. Lett.* **2009**, *95*, 073116.
(23) Li, H.; Misra, A.; Baldwin, J. K.; Picraux, S. T. Synthesis and characterization of nanoporous Pt-Ni alloys. *Appl. Phys. Lett.* **2009**, *95*, 201902.
(24) Zeis, R.; Lei, T.; Sieradzki, K.; Snyder, J.; Erlebacher, J. Catalytic reduction of oxygen and hydrogen peroxide by nanoporous gold. *J. Catal.* **2008**, *253*, 132.
(25) Zeis, R.; Mathur, A.; Fritz, G.; Lee, J.; Erlebacher, J. Platinum-plated nanoporous gold: An efficient, low Pt loading electrocatalyst for PEM fuel cells. *J. Power Sources* **2007**, *165*, 65.
(26) Zielasek, V.; Jurgens, B.; Schulz, C.; Biener, J.; Biener, M. M.; Hamza, A. V.; Baumer, M. Gold catalysts: Nanoporous gold foams. *Angew. Chem., Int. Ed.* **2006**, *45*, 8241.
(27) Biener, J.; Wittstock, A.; Zepeda-Ruiz, L. A.; Biener, M. M.; Zielasek, V.; Kramer, D.; Viswanath, R. N.; Weissmuller, J.; Baumer, M.; Hamza, A. V. Surface-chemistry-driven actuation in nanoporous gold. *Nat. Mater.* **2009**, *8*, 47.
(28) Ahl, S.; Cameron, P. J.; Liu, J.; Knoll, W.; Erlebacher, J.; Yu, F. A comparative plasmonic study of nanoporous and evaporated gold films. *Plasmonics* **2008**, *3*, 13.
(29) Lei, C. H.; Shin, Y.; Magnuson, J. K.; Fryxell, G.; Lasure, L. L.; Elliott, D. C.; Liu, J.; Ackerman, E. J. Characterization of functionalized nanoporous supports for protein confinement. *Nanotechnology* **2006**, *17*, 5531.
(30) Hwang, K.-J.; Cho, D. W.; Lee, J.-W.; Im, C. Preparation of nanoporous TiO2 electrodes using different mesostructured silica templates and improvement of the photovoltaic properties of DSSCs. *New J. Chem.* **2012**, *36*, 2094.
(31) Zhang, J.; Desai, D.; Rosenholm, J. M. Tethered Lipid Bilayer Gates: Toward Extended Retention of Hydrophilic Cargo in Porous Nanocarriers. *Adv. Funct. Mater.* **2014**, *24*, 2352.
(32) Yguerabide, J.; Schmidt, J. A.; Yguerabide, E. E. LATERAL MOBILITY IN MEMBRANES AS DETECTED BY FLUORESCENCE RECOVERY AFTER PHOTOBLEACHING. *Biophys. J.* **1982**, *40*, 69.
(33) Briand, E.; Zach, M.; Svedhem, S.; Kasemo, B.; Petronis, S. Combined QCM-D and EIS study of supported lipid bilayer formation and interaction with pore-forming peptides. *Analyst* **2010**, *135*, 343.
(34) Doshi, D. A.; Dattelbaum, A. M.; Watkins, E. B.; Brinker, C. J.; Swanson, B. I.; Shreve, A. P.; Parikh, A. N.; Majewski, J. Neutron reflectivity study of lipid membranes assembled on ordered nanocomposite and nanoporous silica thin films. *Langmuir* **2005**, *21*, 2865.
(35) Purrucker, O.; Hillebrandt, H.; Adlkofer, K.; Tanaka, M. Deposition of highly resistive lipid bilayer on silicon-silicon dioxide

DOI: 10.1021/acs.jpcb.5b04482
J. Phys. Chem. B XXXX, XXX, XXX−XXX

electrode and incorporation of gramicidin studied by ac impedance spectroscopy. *Electrochim. Acta* **2001**, *47*, 791.
(36) Almeida, P. F. F.; Vaz, W. L. C.; Thompson, T. E. Lateral Diffusion in the Liquid-Phases of Dimyristoylphosphatidylcholine cholesterol lipid bilayers-a free-volume analysis. *Biochemistry* **1992**, *31*, 6739.
(37) Groves, J. T.; Ulman, N.; Boxer, S. G. Micropatterning fluid lipid bilayers on solid supports. *Science* **1997**, *275*, 651.
(38) Kepplinger, C.; Hofer, I.; Steinem, C. Impedance analysis of valinomycin activity in nano-BLMs. *Chem. Phys. Lipids* **2009**, *160*, 109.

DOI: 10.1021/acs.jpcb.5b04482
J. Phys. Chem. B XXXX, XXX, XXX−XXX